Research Article
MODELING OF BOOST AND CUK CONVERTERS AND COMPARISON OF THEIR PERFORMANCE IN MPPT

Okan GÜNGÖR*[1], Halil İbrahim YÜKSEK[2]

[1]*Bayburt University, Department of Electronics and Automation, BAYBURT;* ORCID:0000-0001-5258-1765
[2]*Gümüşhane University, Department of Electrical and Electronics Engineering, GÜMÜŞHANE;*
ORCID:0000-0001-8740-65960

ABSTRACT

The efficiency of photovoltaic (PV) panel systems depends on the structure of the photovoltaic cells and the transfer of energy from the PV panel to load. The focus of this study is energy transfer. The most important component in the energy transfer is maximum power point tracking (MPPT). The MPPT consists of two components: the algorithm for calculation the maximum power and the hardware for power generating. This study investigates how some the DC-DC converters (hardware) impact on the performance of the MPPT under six different environmental conditions by using two different duty cycle calculation methods. Contribution of this study to the literatüre is to analyze the performance of some the DC-DC converters in MPPT by completely eliminating the effect of MPPT algorithms. As a result of this study, while using the Boost converter in MPPT applications, the internal resistance of the PV panel must be equal or smaller than load resistance. However, the Cuk converter can reach to maximum power point in all conditions such as temperature, radiation and load.

Keywords: Circuit linearization, DC-DC converter modelling, state-space averaging, maximum power point tracking (MPPT).

1. INTRODUCTION

Demand for renewable energy as global is increasing rapidly because of population and economic growth. Solar energy is the leading source of the renewable energies. Photovoltaic cells are used to convert this energy into electrical energy. The efficiency of commercially available crystalline silicon-based solar cells is between 15% and 22%. In recent years, an efficiency of 46% with compound based multijunction solar cells has been reached in laboratory conditions [1]. However, this rate is still very low. Therefore, the energy that can convert to electrical energy should be used without the losses. To reduce the losses, the photovoltaic panels must be operated at the maximum power point [2,3].

Generating maximum power from the PV panels is possible by equalizing the converter input equivalent resistance to the PV panel internal resistance [4]. If a random load is connected to the PV panel, a certain amount of power can be generated. In addition, if a load equalled to the internal resistance of the PV panel is connected at certain radiation and temperature, it can also

---

* Corresponding Author: e-mail: okangungor@bayburt.edu.tr, tel: (458) 211 11 52

generate the ma ximum power. However, in case of a change in environmental conditions (radiation, temperature, etc.), it is impossible to generate the maximum power from the PV panel. For this reason, the converters are used to eliminate this state [4]. The duty cycles of the converters are set by using the MPPT algorithm.

In the literature, the MPPT studies have been carried out by using many different converters [5-9]. In these studies, radiation or temperature as a variable have been selected and algorithmic performance analyses have been performed [8,9]. In addition, the selected load values are random. In another study, performance of six different converters (Buck, Boost, Buck-Boost, Cuk, Sepic, Zeta) in MPPT is compared [10]. However, no mathematical model was developed through these studies. In the study, incremental conductance algorithm was used as the MPPT algorithm. In another study, three different converters (Buck, Boost, Buck-Boost) are investigated [11]. Perturb and observe algorithm was used in the study as the MPPT algorithm. In another comprehensive study in the literature, five different algorithms (Perturb and Observe, Incremental Conductance, Fractional Open Circuit Voltage, Ripple Correlation Control, Extremum Seeking Control) and three different converters (Buck, Boost, Buck-Boost) are investigated [12]. Another study that used three different DC-DC converters was carried out by using the neural-network (NN) controller and perturb & observe (P&O) algorithm [4]. However, performance of converters in tracking of maximum power point (MPP) in these studies [4,8 - 12] were not analyzed by completely eliminating the effect of MPPT algorithms. In this study, unlike other studies, it only analyzes the performance of some converters in tracking MPP by completely eliminating the effect of MPPT algorithms.

In the analysis of the converters, six different environmental conditions and two different duty cycle calculation method have been applied. In the first method, the duty cycle is calculated by using the proportional-integral-derivative (PID) controller. The method is completely mathematical. For this reason, the converters are modelled to design the PID controller. Reference for the PID controller is directly obtained from catalog. In the second method, the duty cycle is calculated based on the Perturb and Observe (PNO) algorithm. The PNO algorithm can directly calculate the duty cycle and reach to the MPP without modelling the converters. According to the PNO algorithm, the MPP is point where the derivative of the power with respect to voltage is zero. The PNO algorithm by using a fixed step size changes the duty cycle to reach MPP. The other MPPT algorithms can also reach to the MPP by tracking the power change as mentioned in the PNO algorithm [7,13]. The information about the MPPT algorithms is limited to the information given in this study because there are many studies on the MPPT algorithms in literature [13-16].

2. CRITERIA TO BE CONSIDERED IN THE SELECTION OF CONVERTERS IN MPPT APPLICATIONS

In order to generate maximum power from the PV panels, the internal resistance of the PV panel must be equal to the converter input equivalent resistance. For this purpose, the converter input equivalent resistance is equalized to the internal resistance of the PV panel by observing the duty cycle. The internal resistance of the PV panel (R_{opt}) is constant in a given radiation and temperature. According to Figure 1, the ability of Boost and Cuk converters to reach MPP at different load values is investigated.
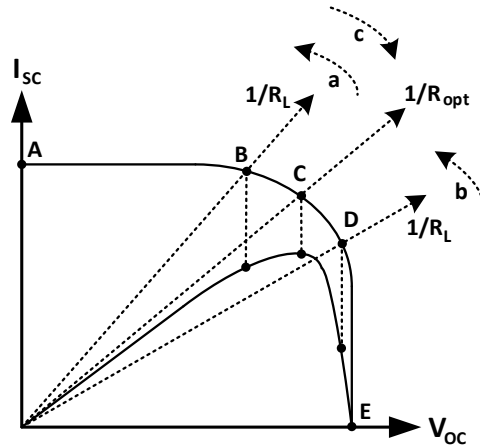
Figure 1. PV panel short circuit current (I_{SC}) x open circuit voltage (V_{OC})

For the Boost converter, the relationship between internal resistance of the PV panel (R_{opt}) and the converter input equivalent resistance (R_L) is defined as follows [17]:

$$R_{opt} = R_L(1-D)^2 \qquad (1)$$

If the duty cycle is equal to zero, the converter input equivalent conductivity ($1/R_L$) given in Figure 1 is at 'A' point. If the converter input equivalent resistance is smaller than the internal resistance of the PV panel and the duty cycle is equal to zero, the slope of the line representing the converter input equivalent conductivity shown in Figure 1 is higher than the slope of the line representing the PV panel internal conductivity. For this reason, the control of duty cycle can be enabled between 'A' and 'B' points in 'a' and 'c' direction. However, since the MPP is the 'C' point, the Boost converter can not reach to the MPP. If the converter input equivalent resistance is greater than the internal resistance of the PV panel and the duty cycle is equal to zero, the slope of the line representing the converter input equivalent conductivity in shown Figure 1 is lower than the slope of the line representing the PV panel internal conductivity. In this case, the control of duty cycle can be enabled between 'A' and 'D' points (including 'C' point) in 'a' and 'c' direction. Because the MPP is 'C' point, the Boost converter can reach to the MPP.

For the Cuk converter, the relationship between the internal resistance of the PV panel and the converter input equivalent resistance is defined as follows [18]:

$$R_{opt} = R_L(\frac{1-D}{D})^2 \qquad (2)$$

If the duty cycle is equal to zero, the converter input equivalent conductivity is at the 'E' point. If the duty cycle is equal to zero, the converter input equivalent conductivity is at the 'A' point. Since 'C' point is between 'A' and 'E' points, the Cuk converter can reach to the MPP in all loads. The losses of inductor, capacitor, diode and switching components that are used in this study are neglect. For this reason, these components are used as ideal for this study in next chapters.

3. MATHEMATICAL MODEL OF BOOST CONVERTER

The Boost converter consists of inductor, capacitor, diode and switching components. Output voltage of the Boost converter is greater than input voltage and output current of the Boost converter is smaller than input current. The block diagram of the Boost converter is shown in Figure 2.
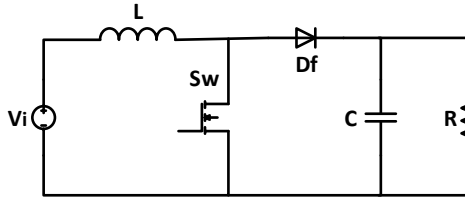

Figure 2. The block diagram of the Boost converter

The parameter values of the Boost converter used in this study are given in Table 1.

Table 1. Parameter values of the Boost converter

Parameter	Value
L	2mH
C	250μF
Switching frequency	50 kHz

The switching states of the Boost converter are shown as below.
Switch on:
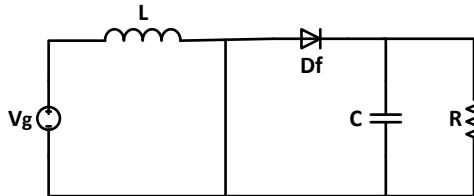
Figure 1. The Boost converter in switch on

$$L\frac{di_L}{dt} = V_g \tag{3}$$

$$C\frac{dV_C}{dt} = -\frac{1}{R}V_C - i_z \tag{4}$$

Equation (5) is obtained by writing the above equations (3, 4) in vector matrix form ($\dot{x} = A_1 x + B_1 u$).

$$\begin{bmatrix} \dot{i}_L \\ \dot{v}_C \end{bmatrix} = \begin{bmatrix} 0 & 0 \\ 0 & -1/RC \end{bmatrix} \begin{bmatrix} i_L \\ V_C \end{bmatrix} + \begin{bmatrix} 1/L \\ 0 \end{bmatrix} [V_g] + \begin{bmatrix} 0 \\ -1/C \end{bmatrix} [i_Z] \tag{5}$$

Switch off:
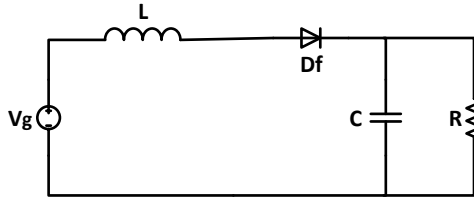
Figure 2. The Boost converter in switch off

$$L \frac{di_L}{dt} = V_g \tag{6}$$

$$C \frac{dV_C}{dt} = -\frac{1}{R} V_C + i_L - i_Z \tag{7}$$

Equation (8) is obtained by writing the above equations (6, 7) in vector matrix form.

$$\begin{bmatrix} \dot{i}_L \\ \dot{v}_C \end{bmatrix} = \begin{bmatrix} 0 & -1/L \\ 1/C & -1/RC \end{bmatrix} \begin{bmatrix} i_L \\ V_C \end{bmatrix} + \begin{bmatrix} 1/L \\ 0 \end{bmatrix} [V_g] + \begin{bmatrix} 0 \\ -1/C \end{bmatrix} [i_Z] \tag{8}$$

For the switch on and switch off situations of the Boost converter, the state equations in given equation (5, 8) are combined to obtain the average large signal model.

$$\begin{aligned} A &= A_1 d + A_2 (1-d) \\ B &= B_1 d + B_2 (1-d) \\ C &= C_1 d + C_2 (1-d) \\ D &= D_1 d + D_2 (1-d) \end{aligned} \tag{9}$$

$$\begin{bmatrix} \dot{i}_L \\ \dot{v}_C \end{bmatrix} = \begin{bmatrix} 0 & -\dfrac{1-d}{L} \\ \dfrac{1-d}{C} & -\dfrac{1}{RC} \end{bmatrix} \begin{bmatrix} i_L \\ v_C \end{bmatrix} + \begin{bmatrix} \dfrac{1}{L} & 0 \\ 0 & -\dfrac{1}{C} \end{bmatrix} \begin{bmatrix} v_g \\ i_Z \end{bmatrix} \tag{10}$$

Obtained the average large signal model is composed of steady state (D) and small signal ($\hat{d}$) model. For the steady state situation, the average large signal model 'd' is changed into 'D', and all other variables are represented by an upper case letter.

$$v_c = V_c + \hat{v}_c \tag{11}$$

$$i_L = I_L + \hat{i}_L \tag{12}$$

$$i_z = I_z + \hat{i}_z \tag{13}$$

$$d = D + \hat{d} \tag{14}$$

$$v_g = V_g + \hat{v}_g \tag{15}$$

In the large signal model, the small signs and steady state signs in given equations (11-15) are put in equation (10) and the equation (16) is obtained.

$$\begin{bmatrix} \overset{\bullet}{I_L + \hat{i}_L} \\ \overset{\bullet}{V_C + \hat{v}_C} \end{bmatrix} = \begin{bmatrix} 0 & -\dfrac{1-D+\hat{d}}{L} \\ \dfrac{1-D+\hat{d}}{C} & \dfrac{1}{RC} \end{bmatrix} \begin{bmatrix} I_L + \hat{i}_L \\ V_C + \hat{v}_C \end{bmatrix} + \begin{bmatrix} \dfrac{1}{L} \\ 0 \end{bmatrix} \begin{bmatrix} V_g + \hat{v}_g \end{bmatrix} + \begin{bmatrix} 0 \\ -\dfrac{1}{C} \end{bmatrix} \begin{bmatrix} I_Z + \hat{i}_z \end{bmatrix} \tag{16}$$

State variables and input variables in the average large signal model are composed of two components which consist of the average values in the operating point and the oscillation values around it.

To obtain a small signal model from the equation (16),

1- $AX + BU = 0$
2- The multiplication of two small signal are supposed that it are zero [19].

$$\begin{bmatrix} \overset{\bullet}{I_L + \hat{i}_L} \\ \overset{\bullet}{V_C + \hat{v}_C} \end{bmatrix} = \underbrace{\begin{bmatrix} 0 & -\dfrac{(1-D)}{L} \\ \dfrac{1-D}{C} & -\dfrac{1}{RC} \end{bmatrix} \begin{bmatrix} I_L \\ V_C \end{bmatrix} + \begin{bmatrix} \dfrac{1}{L} \\ -\dfrac{1}{C} \end{bmatrix} \begin{bmatrix} V_g \\ I_z \end{bmatrix}}_{AX+BU=0}$$

$$+ \underbrace{\begin{bmatrix} 0 & \dfrac{\hat{d}}{L} \\ \dfrac{\hat{d}}{L} & 0 \end{bmatrix} \begin{bmatrix} \hat{i}_L \\ \hat{v}_C \end{bmatrix}}_{0} + \begin{bmatrix} 0 & -\dfrac{\hat{d}}{L} \\ \dfrac{\hat{d}}{C} & 0 \end{bmatrix} \begin{bmatrix} I_L \\ V_C \end{bmatrix} + \begin{bmatrix} 0 & -\dfrac{(1-D)}{L} \\ \dfrac{1-D}{C} & -\dfrac{1}{RC} \end{bmatrix} \begin{bmatrix} \hat{i}_L \\ \hat{v}_C \end{bmatrix} + \begin{bmatrix} \dfrac{1}{L} \\ 0 \end{bmatrix} \begin{bmatrix} \hat{V}_g \end{bmatrix} + \begin{bmatrix} 0 \\ -\dfrac{1}{C} \end{bmatrix} \begin{bmatrix} \hat{i}_z \end{bmatrix} \tag{17}$$

The equation (17) is rearranged below by taking into account the assumptions and equation (18) is obtained.

$$\begin{bmatrix} \overset{\bullet}{\hat{i}_L} \\ \overset{\bullet}{\hat{v}_C} \end{bmatrix} = \begin{bmatrix} 0 & -\dfrac{(1-D)}{L} \\ \dfrac{1-D}{C} & -\dfrac{1}{RC} \end{bmatrix} \begin{bmatrix} \hat{i}_L \\ \hat{v}_C \end{bmatrix} + \begin{bmatrix} \dfrac{1}{L} & 0 & \dfrac{V_C}{L} \\ 0 & -\dfrac{1}{C} & -\dfrac{i_L}{C} \end{bmatrix} \begin{bmatrix} \hat{v}_g \\ \hat{i}_z \\ \hat{d} \end{bmatrix} \tag{18}$$

State equation ($\dot{\hat{x}} = A\hat{x} + B\hat{u}$) is obtained. There are three input signs: Duty cycle ($\hat{d}$), PV panel output voltage ($\hat{v}_g$) and load current ($\hat{i}_z$). In the controller design, the PV panel output voltage and load current changes are taken as zero.

Output equation:

$$\hat{y} = C\hat{x} + D\hat{u} \tag{19}$$

Since the input has directly no effect on the output, $D = 0$.

$$\begin{bmatrix} \hat{v}_0 \\ \hat{i}_i \end{bmatrix} = \begin{bmatrix} 0 & 1 \\ 1 & 0 \end{bmatrix} \begin{bmatrix} \hat{i}_L \\ \hat{v}_C \end{bmatrix} \tag{20}$$

The transfer function of the Boost converter is obtained by using the coefficients matrices of the state equations. The PID controller design is based on the transfer function,

$$\frac{\hat{i}_i}{\hat{d}} = C[sI - A]^{-1}[B] = \frac{1.477e04s + 1.182e07}{s^2 + 400s + 693842} \tag{21}$$

Since PID coefficients design methods are outside the scope of this study, the PID coefficients are obtained by using Matlab interface designs.

$$Kp = 0.0105, \ Ki = 16.2, \ Kd = 1.69e\text{-}06 \tag{22}$$

4. MATHEMATICAL MODEL OF CUK CONVERTER

The inductor, capacitor and resistance are linear circuit elements. These components are modeled by using linear differential equations. But diode and switching components are non-linear. Therefore, linearization has to be done for control. The block diagram of the Cuk converter is shown in the Figure 5.
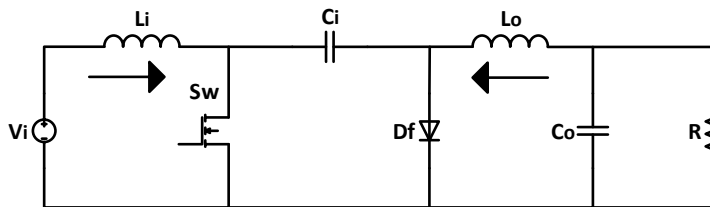

Figure 5. The block diagram of the Cuk converter

The parameter values of the Cuk converter used in this study are given in Table 2.

Table 2. Parameter values of the Cuk converter

Parameter	Value
L_i	5mH
L_o	5mH
C_i	47μF
C_o	1μF
Switching frequency	50 kHz

In the first step for linearization, Cuk converter differential equations are obtained according to two different switching states. Cuk converter state space equations are written in vector matrix form using steady state average value approach [20]. The small signal model of the Cuk converter is used for the operating point determined in the controler design. This model obtained is given below according to the switching status.

Switch on:
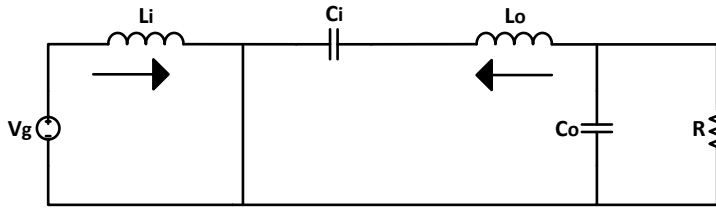
Figure 6. The Cuk converter in switch on

$$L_i \frac{di_{Li}}{dt} = V_g \tag{23}$$

$$L_0 \frac{di_{L0}}{dt} = -V_{Ci} - V_{C0} \tag{24}$$

$$C_i \frac{dV_{Ci}}{dt} = i_{L0} \tag{25}$$

$$C_0 \frac{dV_{C0}}{dt} = i_{L0} - \frac{V_{C0}}{R} \tag{26}$$

Equation (27) is obtained by writing the equations in the form of vector matrix.

$$\begin{bmatrix} \dot{i}_{Li} \\ \dot{i}_{L0} \\ \dot{v}_{Ci} \\ \dot{v}_{C0} \end{bmatrix} = \begin{bmatrix} 0 & 0 & 0 & 0 \\ 0 & 0 & -1/L_0 & -1/L_0 \\ 0 & 1/C_i & 0 & 0 \\ 0 & 1/C_0 & 0 & -1/RC_0 \end{bmatrix} \begin{bmatrix} i_{Li} \\ i_{L0} \\ v_{Ci} \\ v_{C0} \end{bmatrix} + \begin{bmatrix} 1/L_i \\ 0 \\ 0 \\ 0 \end{bmatrix} \begin{bmatrix} v_g \end{bmatrix} + \begin{bmatrix} 0 \\ 0 \\ 0 \\ -1/C_0 \end{bmatrix} \begin{bmatrix} i_Z \end{bmatrix} \tag{27}$$
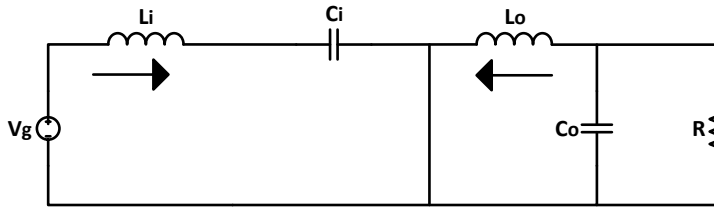
Switch off:

Figure 3. The Cuk converter in switch off

$$L_i \frac{di_{Li}}{dt} = V_g - V_{ci} \tag{28}$$

$$L_0 \frac{di_{L0}}{dt} = -V_{C0} \tag{29}$$

$$C_i \frac{dV_{Ci}}{dt} = i_{Li} \tag{30}$$

$$C_0 \frac{dV_{C0}}{dt} = i_{L0} - \frac{V_{C0}}{R} \tag{31}$$

Equation (32) is obtained by writing the equations in the form of vector matrix.

$$\begin{bmatrix} \dot{i}_{Li} \\ \dot{i}_{L0} \\ \dot{v}_{Ci} \\ \dot{v}_{C0} \end{bmatrix} = \begin{bmatrix} 0 & 0 & -1/L_i & 0 \\ 0 & 0 & 0 & -1/L_0 \\ 1/C_i & 0 & 0 & 0 \\ 0 & 1/C_0 & 0 & -1/RC_0 \end{bmatrix} \begin{bmatrix} i_{Li} \\ i_{L0} \\ v_{Ci} \\ v_{C0} \end{bmatrix} + \begin{bmatrix} 1/L_i \\ 0 \\ 0 \\ 0 \end{bmatrix} [v_g] + \begin{bmatrix} 0 \\ 0 \\ 0 \\ -1/C_0 \end{bmatrix} [i_z] \tag{32}$$

The average large signal model is obtained by combining the state equations in given equation (27, 32) for the Cuk converter's switch on and switch off situations.

$$\begin{aligned} A &= A_1 d + A_2(1-d) \\ B &= B_1 d + B_2(1-d) \\ C &= C_1 d + C_2(1-d) \\ D &= D_1 d + D_2(1-d) \end{aligned} \tag{33}$$

$$
\begin{bmatrix} \dot{i}_{Li} \\ \dot{i}_{L0} \\ \dot{v}_{Ci} \\ \dot{v}_{C0} \end{bmatrix} =
\begin{bmatrix}
0 & 0 & -(\dfrac{1-d}{L_i}) & 0 \\
0 & 0 & -\dfrac{d}{L_0} & \dfrac{-d+d-1}{L_0} \\
\dfrac{1-d}{C_i} & \dfrac{d}{Ci} & 0 & 0 \\
0 & \dfrac{d+1-d}{C_0} & 0 & \dfrac{-d+d-1}{RC_0}
\end{bmatrix}
\begin{bmatrix} i_{Li} \\ i_{L0} \\ v_{Ci} \\ v_{C0} \end{bmatrix} +
$$

$$
\begin{bmatrix} \dfrac{d}{L_i} \\ 0 \\ 0 \\ 0 \end{bmatrix} [v_g] +
\begin{bmatrix} \dfrac{1-d}{L_i} \\ 0 \\ 0 \\ 0 \end{bmatrix} [v_g] +
\begin{bmatrix} 0 \\ 0 \\ 0 \\ -d/C_0 \end{bmatrix} [i_z] +
\begin{bmatrix} 0 \\ 0 \\ 0 \\ d-1/C_0 \end{bmatrix} [i_z] \tag{34}
$$

Obtained the average large signal model is composed of steady state (D) and small signal ($\hat{d}$) model. For the steady state situation, the average large signal model 'd' is changed into 'D', and all other variables are represented by an upper case letter.

$$d = D + \hat{d} \tag{35}$$

$$v_{C0} = V_{C0} + \hat{v}_{C0} \tag{36}$$

$$v_{Ci} = V_{Ci} + \hat{v}_{ci} \tag{37}$$

$$v_g = V_g + \hat{v}_g \tag{38}$$

$$i_Z = I_Z + \hat{i}_Z \tag{39}$$

$$i_{Li} = I_{Li} + \hat{i}_{Li} \tag{40}$$

$$i_{L0} = I_{L0} + \hat{i}_{L0} \tag{41}$$

In the large signal model, the small signs and steady state signs in given equations (35-41) are put in equation (34) and the equation (42) is obtained.

$$
\begin{bmatrix}
\overset{\bullet}{I_{Li}+\hat{i}_{Li}} \\[6pt]
\overset{\bullet}{I_{L0}+\hat{i}_{L0}} \\[6pt]
\overset{\bullet}{V_{Ci}+\hat{v}_{Ci}} \\[6pt]
\overset{\bullet}{V_{C0}+\hat{v}_{C0}}
\end{bmatrix}
=
\begin{bmatrix}
0 & 0 & \dfrac{D+\hat{d}-1}{L_i} & 0 \\[10pt]
0 & 0 & \dfrac{-D-\hat{d}}{L_0} & -\dfrac{1}{L_0} \\[10pt]
\dfrac{-D-\hat{d}+1}{C_i} & \dfrac{+D+\hat{d}}{C_i} & 0 & 0 \\[10pt]
0 & \dfrac{1}{C_0} & 0 & -\dfrac{1}{RC_0}
\end{bmatrix}
\begin{bmatrix}
I_{Li}+\hat{i}_{Li} \\[6pt]
I_{L0}+\hat{i}_{L0} \\[6pt]
V_{Ci}+\hat{v}_{Ci} \\[6pt]
V_{C0}+\hat{v}_{C0}
\end{bmatrix}
+
\begin{bmatrix}
\dfrac{1}{L_i} & 0 \\[10pt]
0 & 0 \\[10pt]
0 & 0 \\[10pt]
0 & \dfrac{-1}{C_0}
\end{bmatrix}
\begin{bmatrix}
V_g+\hat{v}_g \\[6pt]
I_z+\hat{i}_z
\end{bmatrix}
\tag{42}
$$

State variables in the large signal model ($i_{L1},i_{L2},v_{Ci},v_{C0}$) and input variables ($v_g,i_z,d$) consists of two components which consist of the average value in the operation point and the oscillation around it.

To obtain a small signal model from equation (42),

1- $AX+BU=0$

2- It is supposed that the multiplication of two small signals is zero [19].

$$
\begin{bmatrix}
\overset{\bullet}{\hat{i}_{Li}} \\[6pt]
\overset{\bullet}{\hat{i}_{L0}} \\[6pt]
\overset{\bullet}{\hat{v}_{Ci}} \\[6pt]
\overset{\bullet}{\hat{v}_{C0}}
\end{bmatrix}
=
\underbrace{
\begin{bmatrix}
0 & 0 & \dfrac{D-1}{L_i} & 0 \\[10pt]
0 & 0 & -\dfrac{D}{L_0} & -\dfrac{1}{L_0} \\[10pt]
\dfrac{1-D}{C_i} & \dfrac{D}{C_i} & 0 & 0 \\[10pt]
0 & \dfrac{1}{C_0} & 0 & -\dfrac{1}{RC_0}
\end{bmatrix}
\begin{bmatrix}
I_{Li} \\[6pt]
I_{L0} \\[6pt]
V_{Ci} \\[6pt]
V_{C0}
\end{bmatrix}
+
\begin{bmatrix}
\dfrac{1}{L_i} & 0 \\[10pt]
0 & 0 \\[10pt]
0 & 0 \\[10pt]
0 & \dfrac{-1}{C_0}
\end{bmatrix}
\begin{bmatrix}
V_g \\[6pt]
I_z
\end{bmatrix}
}_{AX+BU=0}
+
$$

$$
\underbrace{
\begin{bmatrix}
0 & 0 & \dfrac{\hat{d}}{L_i} & 0 \\[10pt]
0 & 0 & -\dfrac{\hat{d}}{L_0} & 0 \\[10pt]
-\dfrac{\hat{d}}{C_i} & \dfrac{\hat{d}}{C_i} & 0 & 0 \\[10pt]
0 & 0 & 0 & 0
\end{bmatrix}
\begin{bmatrix}
\hat{i}_{Li} \\[6pt]
\hat{i}_{L0} \\[6pt]
\hat{v}_{Ci} \\[6pt]
\hat{v}_{C0}
\end{bmatrix}
}_{0}
+
\begin{bmatrix}
0 & 0 & \dfrac{D-1}{L_i} & 0 \\[10pt]
0 & 0 & -\dfrac{D}{L_0} & -\dfrac{1}{L_0} \\[10pt]
\dfrac{1-D}{C_i} & \dfrac{D}{C_i} & 0 & 0 \\[10pt]
0 & \dfrac{1}{C_0} & 0 & -\dfrac{1}{RC_0}
\end{bmatrix}
\begin{bmatrix}
\hat{i}_{Li} \\[6pt]
\hat{i}_{L0} \\[6pt]
\hat{v}_{Ci} \\[6pt]
\hat{v}_{C0}
\end{bmatrix}
$$

$$
+
\begin{bmatrix}
0 & 0 & \dfrac{\hat{d}}{L_i} & 0 \\[10pt]
0 & 0 & -\dfrac{\hat{d}}{L_0} & 0 \\[10pt]
-\dfrac{\hat{d}}{C_i} & \dfrac{\hat{d}}{C_i} & 0 & 0 \\[10pt]
0 & 0 & 0 & 0
\end{bmatrix}
\begin{bmatrix}
I_{Li} \\[6pt]
I_{L0} \\[6pt]
V_{Ci} \\[6pt]
V_{C0}
\end{bmatrix}
+
\begin{bmatrix}
\dfrac{1}{L_i} & 0 \\[10pt]
0 & 0 \\[10pt]
0 & 0 \\[10pt]
0 & \dfrac{-1}{C_0}
\end{bmatrix}
\begin{bmatrix}
\hat{v}_g \\[6pt]
\hat{i}_z
\end{bmatrix}
\tag{43}
$$

The equation (43) is rearranged below by taking into account the assumptions and equation (44) is obtained.

$$
\begin{bmatrix} \dot{\hat{i}}_{Li} \\ \dot{\hat{i}}_{L0} \\ \dot{\hat{v}}_{Ci} \\ \dot{\hat{v}}_{C0} \end{bmatrix} = \underbrace{\begin{bmatrix} 0 & 0 & \dfrac{D-1}{L_i} & 0 \\ 0 & 0 & -\dfrac{D}{L_0} & -\dfrac{1}{L_0} \\ \dfrac{1-D}{C_i} & \dfrac{D}{C_i} & 0 & 0 \\ 0 & \dfrac{1}{C_0} & 0 & -\dfrac{1}{RC_0} \end{bmatrix}}_{A\hat{x}} \begin{bmatrix} \hat{i}_{Li} \\ \hat{i}_{L0} \\ \hat{v}_{Ci} \\ \hat{v}_{C0} \end{bmatrix} + \underbrace{\begin{bmatrix} \dfrac{V_{Ci}}{L_i} \\ -\dfrac{V_{Ci}}{L_0} \\ \dfrac{-I_{Li}+I_{L0}}{C_i} \\ 0 \end{bmatrix} [\hat{d}]}_{B_1\hat{U}} + \underbrace{\begin{bmatrix} \dfrac{1}{L_i} \\ 0 \\ 0 \\ 0 \end{bmatrix} [\hat{v}_g]}_{B_2\hat{U}} + \underbrace{\begin{bmatrix} 0 \\ 0 \\ 0 \\ -\dfrac{1}{RC_0} \end{bmatrix} [\hat{i}_Z]}_{B_3\hat{U}} \tag{44}
$$

State equation ($\dot{\hat{x}} = A\hat{x} + B\hat{u}$) is obtained. There are three input signs: duty cycle ($\hat{d}$), panel output voltage ($\hat{v}_g$) and load current ($\hat{i}_z$). In the controller design, the panel output voltage and load current changes are taken to zero.

Output equation:

$$
\hat{y} = C\hat{x} + D\hat{u} \tag{45}
$$

Since the input has no effect on the output, $D = 0$.

$$
\begin{bmatrix} \hat{v}_0 \\ \hat{i}_i \end{bmatrix} = \underbrace{\begin{bmatrix} 0 & 0 & 0 & 1 \\ 1 & 0 & 0 & 0 \end{bmatrix} \begin{bmatrix} \hat{i}_{Li} \\ \hat{i}_{L0} \\ \hat{v}_{Ci} \\ \hat{v}_{C0} \end{bmatrix}}_{C\hat{x}} + \underbrace{\begin{bmatrix} 0 & 0 \end{bmatrix}}_{D\hat{u}} \tag{46}
$$

The transfer function of the Cuk converter is obtained by using the coefficients matrices of the state equations. The PID controller design is based on the transfer function.

$$
\frac{\hat{i}_i}{\hat{d}} = C[sI-A]^{-1}[B] = \frac{9200s^3 + 9.232e08s^2 + 2.185e12s + 3.103e15}{s^4 + 1e05s^3 + 2.023e08s^2 + 2.269e11s + 1.171e14} \tag{47}
$$

Since PID coefficients design methods are out of the scope of this study, PID coefficients were obtained by using Matlab interface designs.

$$
\text{Kp} = 0.074, \ \text{Ki} = 39.9, \ \text{Kd} = 4.19e-06 \tag{48}
$$

5. SIMULATION RESULTS

In the previous sections, the mathematical model of Cuk and Boost converters was obtained and the PID controllers were designed. In this section, performances of Boost and Cuk converters are analyzed under different conditions such as radiation, temperature and load. The duty cycle is calculated in two different ways for the operation of converters. In the first, the current at MPP (I_{MPP}) value of the PV panel under the specified conditions is taken from the catalog. This I_{MPP}

value is used as reference (I_{REF}) for PID controller. The current of PV panel (I_{PV}) is measured and the duty cycle of converters is calculated by PID controller. In the second, controller are not designed and duty cycle is calculated by the PNO algorithm that based on the measurement of the PV panel current (I_{PV}) and voltage (V_{PV}). The step size of the PNO algorithm is 0.01. The algorithm performs a measurement of every 0.02s.

The first method is completely deterministic, but it is not applicable in real applications because it is very difficult to find an I_{MPP} value by measuring continuous environmental conditions. Therefore, this method is used exclusively for this study. The second method contains no deterministic operations and it focuses only on monitoring the system.

The block diagram of the system generated in the Matlab / Simulink program is given in Figure 8.
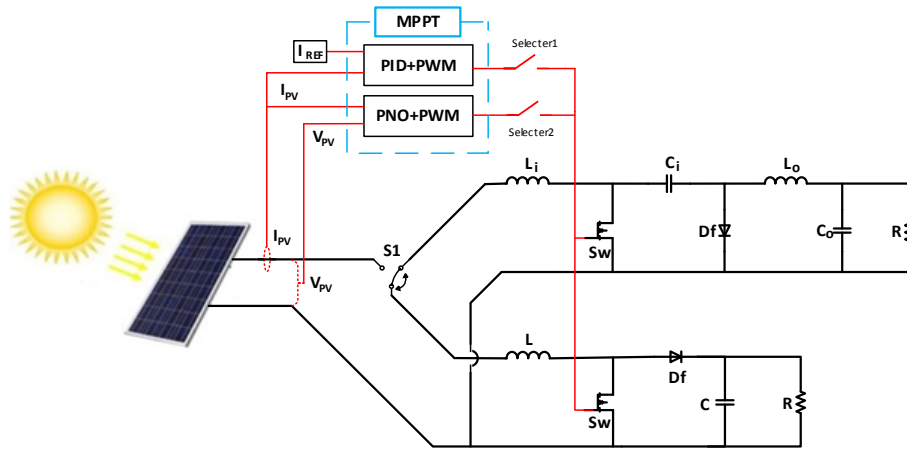
Figure 8. MPPT block diagram

The signal as given reference current is the current value at the maximum point of the PV panel. Electrical characteristics of the PV panel that is used in this study are shown in Table 3[21].

Table 3. The PV panel characteristics in STC (STC refers to temperature of 25°C and irradiation of 1000 W/m².)

Electrical performance of KC85T	Value
Power at MPP (Pmax)	87.35 W
Voltage at MPP (Vmpp)	17.4 V
Current at MPP (Impp)	5.02 A
Open Circuit Voltage (Voc)	21.7 V
Short Circuit Current (Isc)	5.35 A

When the environmental conditions change, the internal resistance of the PV panel changes. Radiation-panel internal resistance and temperature-panel internal resistance curves of KC85T panel are presented in Figure 9 and Figure 10, respectively.
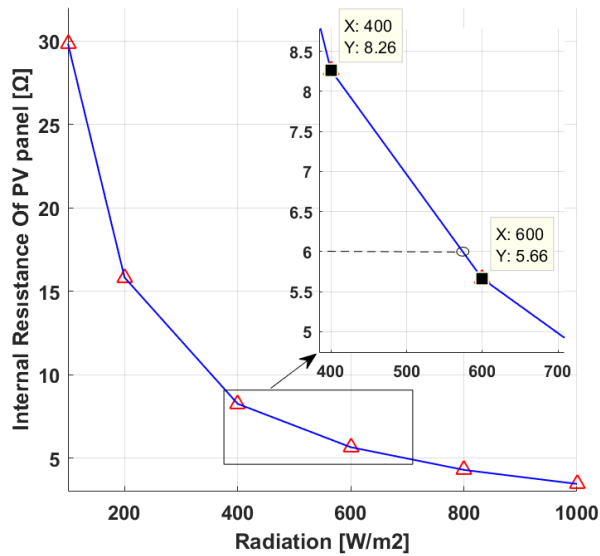
**Figure 9.** Internal resistance of PV panel-radiation
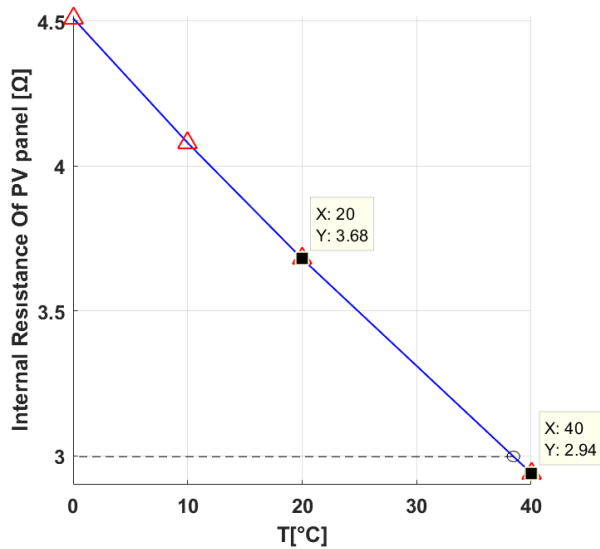
Figure 10. Internal resistance of PV panel-temperature

The important factors about the choice of converter in PV systems were mentioned in the second chapter. These factors are studied at the cases 1, 2, 3 and 4.

Case 1: Radiation: 600 W/m² (0s – 2s) - 400 W/m² (2s – 4s), Load: 6 ohms, Temperature: 25°C
Converter: Boost converter
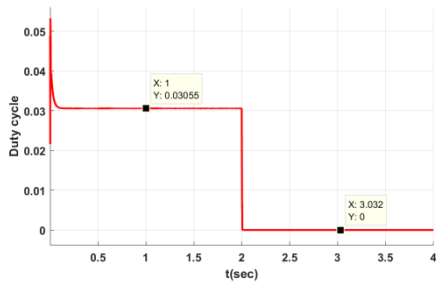
**Figure 11.** Calculation of duty cycle by using PID   **Figure 12.** Output power of PV when using PID
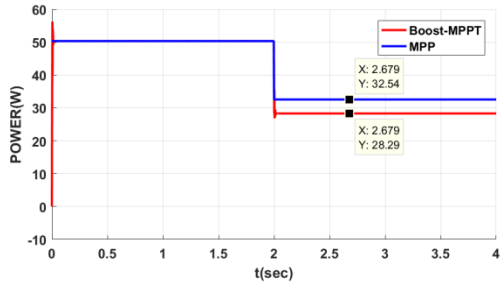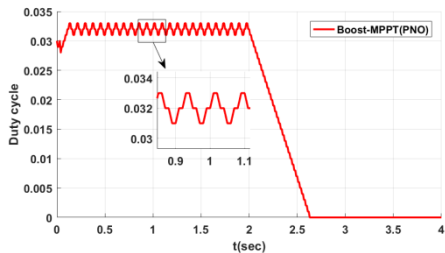
Figure 13. Calculation of duty cycle by using PNO **Figure 14.** Output power of PV when using PNO
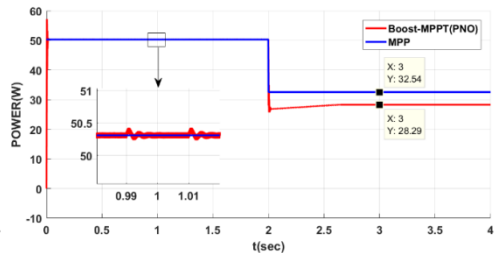
In case 1, radiation is variable while temperature and load are constant. In the range of 0-2s, the internal resistance of the PV panel (5.66 ohms) is less than the Boost converter input equivalent resistance (6 ohms). For this reason, the Boost converter can reach to the MPP by using both the PID controller and the PNO algorithm. In the range of 2-4s, the internal resistance of the PV panel (8.26 ohms) is greater than the Boost converter input equivalent resistance (6 ohms). In this period of time, the Boost converter can not reach to the MPP by using both the PID controller and the PNO algorithm. The duty cycle calculated using the PID controller and PNO algorithm is shown in Figure 11 and Figure 13, respectively.

The Boost converter can only transfer of 28.29 W to the load as shown in Figure 12 and Figure 14. But, the MPP of PV panel is 32.54 W. So the efficiency is 86%.

Case 2: Radiation: 1000 W/m², Load: 3 ohms, Temperature: 40°C (0s – 2s) - 20°C (2s – 4s)
Converter: Boost converter
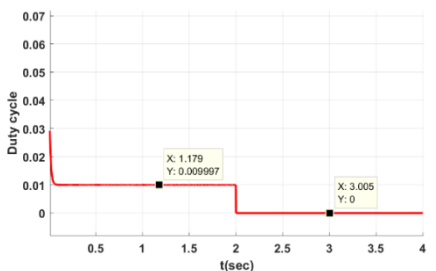
Figure 15. Calculation of duty cycle by using PID   **Figure 16.** Output power of PV when using PID
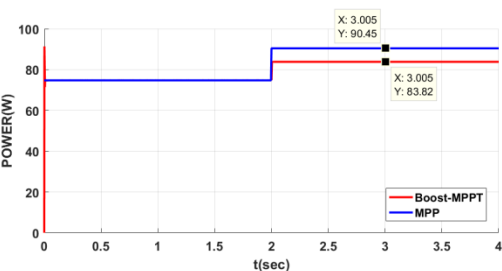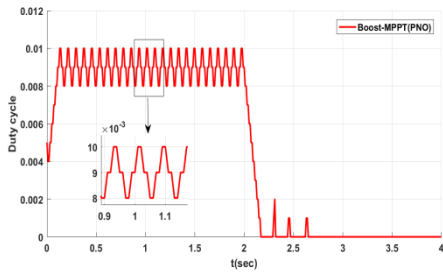
Figure 17. Calculation of duty cycle by using PNO   **Figure 18.** Output power of PV when using PNO
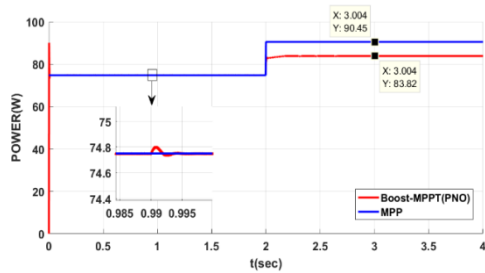
In case 2, temperature is variable while radiation and load are constant. In the range of 0-2s, the internal resistance of the PV panel (2.94 ohms) is less than the Boost converter input equivalent resistance (3 ohms). For this reason, the Boost converter can reach to the MPP by using both the PID controller and the PNO algorithm. In the range of 2-4s, due to decreasing temperature, the internal resistance of the PV panel rise to 3.68 ohms. So the internal resistance of the PV panel is greater than the Boost converter input equivalent resistance (3 ohms). In this period of time, the Boost converter can not reach to the MPP by using both the PID controller and the PNO algorithm. The duty cycle calculated using the PID controller and PNO algorithm is shown in Figure 15 and Figure 17, respectively.

The Boost converter can only transfer of 83.82 W to the load as shown in Figure 16 and Figure 18. But, the MPP of PV panel is 90.45 W. There is of 6.63 W loss. The power loss in both case 1 and case 2 is only due to the converter.

Case 3: Radiation: 600 W/m² (0s - 2s) - 400 W/m² (2s - 4s), Load: 6 ohms, Temperature: 25°C
Converter: Cuk converter
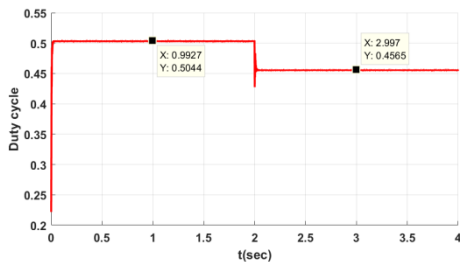
**Figure 19.** Calculation of duty cycle by using PID   **Figure 20.** Output power of PV when using PID
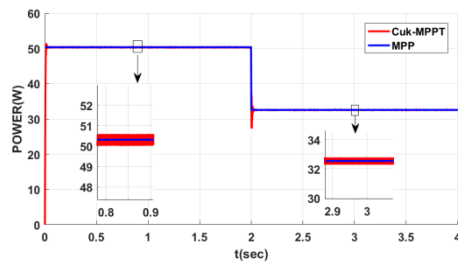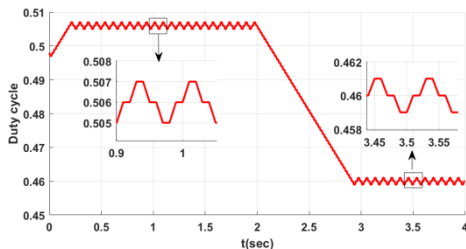
Figure 21. Calculation of duty cycle by using PNO   **Figure 22.** Output power of PV when using PNO
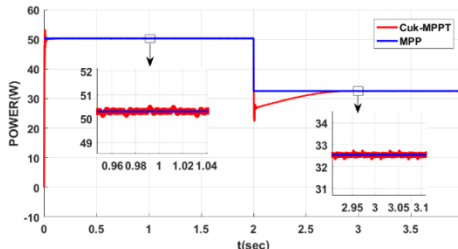
Case 4: Radiation: 1000 W/m², Load: 3 ohms, Temperature: 40°C (0s – 2s) - 20°C (2s – 4s)
Converter: Cuk converter
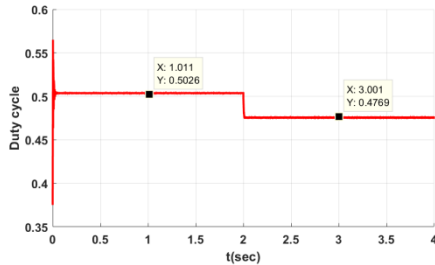
Figure 23. Calculation of duty cycle by using PID
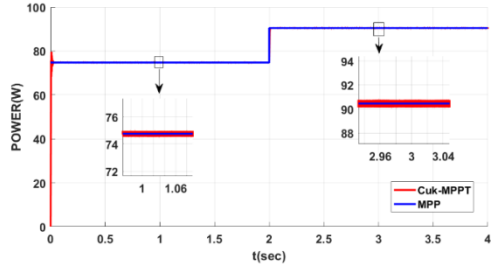
**Figure 24.** Output power of PV when using PID
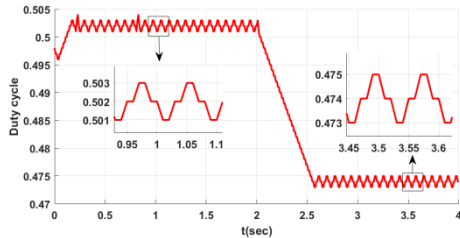
Figure 25. Calculation of duty cycle by using PNO
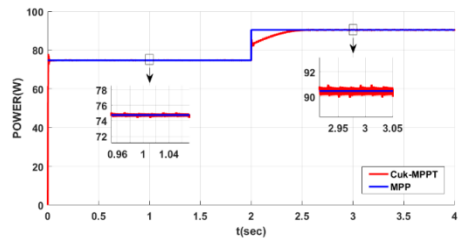
Figure 26. Output power of PV when using PNO

In case 3 and case 4, the Cuk converter tracks MPP without affected from enviromental conditions such as radiation, temperature and variable load while calculating duty cycle by using both PID and PNO methods. Although case 1 and case 2 is are same as case 3 and case 4 in terms of enviromental conditions, the output power of the PV panel is different because of converters. In case 1, 2, 3 and 4, performance of the used converters in MPPT is shown in Table 4.

Table 4. Performance of the converters

Temperature	Radiation	PV panel internal resistance	Load	Cuk MPPT Performance	Boost MPPT Performance
25C°	400W/m²	8.26 Ω	6 Ω	✔	✘
				✔	✘
	600W/m²	5.66 Ω		✔	✔
				✔	✔
40C°	1000W/m²	2.94 Ω	3 Ω	✔	✘
				✔	✘
20C°		3.68 Ω		✔	✔
				✔	✔

6. CONCLUSION

In this study, the MPP tracking performances of Boost and Cuk converters are investigated. The system is simulated on MATLAB/Simulink platform. While investigating these performances, it should be determined that environmental conditions and duty cycle calculation

methods are very important. Therefore, six different environmental conditions and two different duty cycle calculation methods are used. In the calculation of duty cycle of the converters, the PID based method which is completely mathematical and the PNO algorithm based on observation are used. The both duty cycle calculation methods have same response under the different environmental conditions. The performance of the converters in MPPT is clearly shown in Table 4. According to Table 4, the Cuk converter can reach to the MPP in each case whereas the Boost converter can reach to the MPP only at greater the load resistance than the PV panel internal resistance.

REFERENCES

[1]   Dimroth, F., Tibbits, T. N., Niemeyer, M., Predan, F., Beutel, P., Karcher, C., ... & Bett, A. W. (2015). Four-junction wafer-bonded concentrator solar cells. IEEE Journal of Photovoltaics, 6(1), 343-349.

[2]   Mohapatra, A., Nayak, B., & Mohanty, K. B. (2014, December). Current based novel adaptive P&O MPPT algorithm for photovoltaic system considering sudden change in the irradiance. In 2014 IEEE International Conference on Power Electronics, Drives and Energy Systems (PEDES) (pp. 1-4). IEEE.

[3]   Mohapatra, A., Nayak, B., Das, P., & Mohanty, K. B. (2017). A review on MPPT techniques of PV system under partial shading condition. Renewable and Sustainable Energy Reviews, 80, 854-867.

[4]   Nayak, B., Mohapatra, A., & Mohanty, K. B. (2017). Selection criteria of dc-dc converter and control variable for MPPT of PV system utilized in heating and cooking applications. Cogent Engineering, 4(1), 1363357.

[5]   Vivek, P., Ayshwarya, R., Amali, S. J., & Sree, A. N. (2016, April). A novel approach on MPPT algorithm for solar panel using buck boost converter. In 2016 International Conference on Energy Efficient Technologies for Sustainability (ICEETS) (pp. 396-399). IEEE.

[6]   Shaw, P. (2019). Modelling and analysis of an analogue MPPT-based PV battery charging system utilising dc–dc boost converter. IET Renewable Power Generation.

[7]   Radjai, T., Rahmani, L., GAUBERT, J., & Gassab, S. (2014). Fuzzy Logic Variable Step of P&O MPPT with Direct Control Method Using Cuk Converter. In Proc. 11th International Conference On Modeling and Simulation of Electric Machines, Converters and Systems, Valencia, Spain, ELECTRIMACS-2014 (pp. 324-329).

[8]   Singh, S. P., Gautam, A. K., Tripathi, S. P., & Kumar, B. (2017, February). Performance comparison of MPPT techniques using Cuk converter for photovoltaic energy conversion system. In 2017 3rd International Conference on Computational Intelligence & Communication Technology (CICT) (pp. 1-6). IEEE.

[9]   Yadav, A. P. K., Thirumaliah, S., Haritha, G., & Scholar, P. G. (2012). Comparison of mppt algorithms for dc-dc converters based pv systems. International Journal of Advanced Research in Electrical, Electronics and Instrumentation Engineering, 1(1), 18-23.

[10]   Ramki, T., & Tripathy, L. N. (2015, January). Comparison of different DC-DC converter for MPPT application of photovoltaic system. In International Conference on Electrical, Electronics, Signals, Communication and Optimization (EESCO) (pp. 1-6).

[11]   Ba, A., Ehssein, C. O., Mahmoud, M. E. M. O. M., Hamdoun, O., & Elhassen, A. (2018). Comparative Study of Different DC/DC Power Converter for Optimal PV System Using MPPT (P&O) Method. Applied Solar Energy, 54(4), 235-245.

[12]   Shadlu, M. S.   (2019). Comparison of Maximum Power Point Tracking (MPPT) Algorithms to Control DC-DC Converters in Photovoltaic Systems. Recent Advances in Electrical & Electronic Engineering (Formerly Recent Patents on Electrical & Electronic Engineering), 12(4), 355-367.

[13]   Macaulay, J., & Zhou, Z. (2018). A Fuzzy Logical-Based Variable Step Size P&O MPPT Algorithm for Photovoltaic System. Energies, 11(6), 1340.

[14]   Agwa, A. M., & Mahmoud, I. Y. (2017). Photovoltaic Maximum Power Point Tracking by Artificial Neural Networks. Journal of Multidisciplinary Engineering Science and Technology (JMEST), 4(1).

[15]   Kumar, M., Kapoor, S. R., Nagar, R., & Verma, A. (2015). Comparison between IC and fuzzy logic MPPT algorithm based solar PV system using boost converter. International Journal of Advanced Research in Electrical, Electronics and Instrumentation Engineering, 4(6), 4927-4939.

[16]   Radjai, T., Rahmani, L., Mekhilef, S., & Gaubert, J. P. (2014). Implementation of a modified incremental conductance MPPT algorithm with direct control based on a fuzzy duty cycle change estimator using dSPACE. Solar Energy, 110, 325-337.

[17]   Kotak, V. C., & Tyagi, P. (2013). DC to DC Converter in maximum power point tracker. International Journal of Advanced Research in Electrical, Electronics and Instrumentation Engineering, 2(12), 6115-6125.

[18]   Seyedmahmoudian, M., Horan, B., Rahmani, R., Maung Than Oo, A., & Stojcevski, A. (2016). Efficient photovoltaic system maximum power point tracking using a new technique. Energies, 9(3), 147.

[19]   Forsyth, A. J., & Mollov, S. V. (1998). Modelling and control of DC-DC converters. Power engineering journal, 12(5), 229-236.

[20]   Middlebrook, R. D., & Cuk, S. (1976, June). A general unified approach to modelling switching-converter power stages. In 1976 IEEE Power Electronics Specialists Conference (pp. 18-34). IEEE.

[21]   Internet: Energy Matter, URL: https://www.energymatters.com.au/kyocera-85watt-12volt-multicrystal-photovoltaic-module-p-866.html Last Accessed on: 05.05.2020